# Noncovalent Interaction Analysis in Fluctuating Environments

Pan Wu, Robin Chaudret, Xiangqian Hu, and Weitao Yang*

Department of Chemistry, Duke University, Durham, North Carolina 27708, United States

ABSTRACT: Noncovalent interactions play a central role in many chemical and biological systems. In a previous study, Johnson et al. developed a noncovalent interaction (NCI) index to characterize and visualize different types of weak interactions. To apply the NCI analysis to fluctuating environments as in the solution phase, we here developed a new averaged noncovalent interaction (i.e., aNCI) index along with a fluctuation index to characterize the magnitude of interactions and fluctuations. We applied aNCI for various systems including solute−solvent and ligand−protein noncovalent interactions. For water and benzene molecules in aqueous solution, solvation structures and the specific hydrogen bond patterns were visualized clearly. For the $Cl^- + CH_3Cl$ S_N2 reaction in aqueous solution, charge reorganization influences over solvation structure along S_N2 reaction were revealed. For ligand−protein systems, aNCI can recover several key fluctuating hydrogen bond patterns that have potential applications for drug design. Therefore, aNCI, as a complementary approach to the original NCI method, can extract and visualize noncovalent interactions from thermal noise in fluctuating environments.

Fluctuating environment

$$\overline{s(r)} = \frac{1}{2(3\pi^2)^{1/3}} \frac{\overline{|\nabla\rho(r)|}}{\overline{\rho(r)}^{4/3}}$$
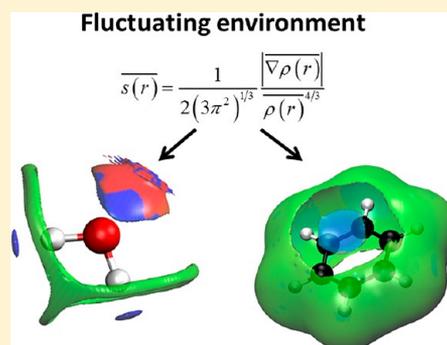
1. INTRODUCTION

Noncovalent interactions play a predominant role in chemistry and biochemistry.[1,2] For instance, such interactions are the driving force to fold[3] and stabilize protein structures,[4] to coil the DNA into a double helix, and to self-assemble molecules.[5] In our previous studies[6,7] a novel noncovalent interaction (NCI) index was proposed to characterize NCI and estimate their strength. This index is a valuable tool to study weak interaction within biological systems.[8,9] Using a promolecular[10,11] density, NCI can characterize large systems with low computational cost and with insightful results. NCI was also applied to metal complexes[12,13] and visualized binding modes of the cations. Influence of noncovalent interactions on the reaction mechanism was also investigated in several studies[8,14] using the NCI analysis. For instance, Gillet et al.[15] showed that an interpretative analysis crossing Electron Localization Function (ELF) and NCI results could allow following every step of a reaction mechanism to reveal reaction details. Finally Contreras-García et al.[7] linked the NCI index with the interaction energy for the specific case of hydrogen bonding. In this study they proposed a scheme to integrate the density on the NCI surfaces and showed that, using this approach, the NCI integrated density could give accurate estimation of the interaction energy. This study made a first quantitative link between NCI analysis and interaction energy.

One limitation of the NCI analysis is that the noncovalent interactions are characterized based on one single structure. However, geometric fluctuations are constantly present in practical molecular systems. For example, in solutions, the positions of solvent molecules fluctuate and the solvent molecules change between solvation shells, which play important roles in solvation and chemical reactions. As such, the application of the NCI index for fluctuating systems is still unclear. In this work, we developed an averaged noncovalent interaction index (aNCI), which uses an ensemble of the structures, to overcome this problem.

This paper is organized as follows: In the next section, we briefly review the NCI analysis and introduce the aNCI analysis. We also explain how aNCI can be readily combined with classical or QM/MM simulations such as the QM/MM-MFEP (Quantum Mechanics/Molecular Mechanics Minimum Free-Energy Path[16,17]) method. In Section 3, we provide the details of simulations and model systems. In Section 4, we elucidate how to choose between different averaged reduced density gradient definitions. Then, using the aNCI index and fluctuation index, we scrutinize three cases, including solvation structures, an S_N2 reaction, and ligand−protein binding environments. We demonstrate the strength and robustness of aNCI analysis to characterize noncovalent interactions in fluctuating systems. Finally, we conclude our works in Section 5.

2. THEORETICAL METHOD

2.1. Brief Review of NCI Analysis. To reveal the weak interactions, Johnson et al.[6] constructed the NCI index based on the study of reduced density gradient (RDG or s) as a function of electron density $\rho(\mathbf{r})$:

$$s(\mathbf{r}) = \frac{1}{2(3\pi^2)^{1/3}} \frac{|\nabla\rho(\mathbf{r})|}{\rho(\mathbf{r})^{4/3}} \tag{1}$$

By plotting RDG with respect to electron density, noncovalent interaction regions can be identified when the RDG approaches zero. The spikes which appear in the 2D plot are associated

Table 1. Model Systems for aNCI Analysis

	solute−solvent system		S_N2 reaction in solvent		ligand−protein system	
subsystem	H_2O	benzene	reactant state	transition state	BIIB021	VHD
environment	water	water	water	water	protein, water	protein, water
cubic box length	40	40	50	50	70	70

with the interaction of critical points (ICP). These ICP regions with both low density and gradient of the density can be visualized in three-dimensional (3D) grid space, which reveals where noncovalent interactions occur. Moreover, based on the analysis of sign(λ_2) (where λ_2 is the second eigenvalue of the density Hessian matrix $\partial\rho(\mathbf{r})/\partial x_i \partial x_j$, with i, j = 1, 2, 3, and x_i representing one Cartesian direction), attractive (negative sign) and repulsive (positive sign) interaction regions can be identified (as previously exposed[6]). As such, with visualization tools, such as VMD,[18] the interaction regions in 3D space can be visualized and colored depending on effective density (sign(λ_2)$\rho(\mathbf{r})$). The following color codes are employed to distinguish interaction types in NCI:

- Blue for the highly attractive interactions (such as hydrogen bonds)
- Green for the weak interactions (such as dispersive-like van der Waals)
- Red for repulsive interactions (such as steric clashes)

2.2. aNCI Analysis. The above NCI analysis has been useful to study weak interactions within static structures. However, in order to analyze noncovalent interactions in thermally fluctuating systems, for instance, trajectories generated from molecular dynamics simulations, a new definition of NCI index is required. Here, we consider two possible definitions of averaging reduced density gradient (aRDG):

Definition a: using averaged density $\overline{\rho(\mathbf{r})}$ and averaged density gradient $\overline{\Delta\rho(\mathbf{r})}$, one can define

$$\overline{s(\mathbf{r})} = \frac{1}{2(3\pi^2)^{1/3}} \frac{|\overline{\nabla\rho(\mathbf{r})}|}{\overline{\rho(\mathbf{r})}^{4/3}} \qquad (2)$$

Definition b: using RDG of each single structure, one can define

$$\langle s(\mathbf{r}) \rangle = \sum_{i=1}^{N_{snapshots}} s_i(\mathbf{r})/N_{snapshots} \qquad (3)$$

$$s_i(\mathbf{r}) = \frac{1}{2(3\pi^2)^{1/3}} \frac{|\nabla\rho_i(\mathbf{r})|}{\rho_i(\mathbf{r})^{4/3}}$$

We will scrutinize both definitions in Section 4.1.1.

To illustrate how thermal motions can affect the weak interactions, we define the thermal fluctuation index as

$$f(\mathbf{r}) = \frac{\text{std}(\{\rho_i(\mathbf{r})\})}{\text{mean}(\{\rho_i(\mathbf{r})\})} \qquad (4)$$

where $\rho_i(\mathbf{r})$ is the electron density from structure i.

The color codes for fluctuation index f are

- Blue for highly stable interactions, which can be barely affected by thermal motions
- Red for flexible interactions, which can be easily distorted by thermal motions
- Green for fluctuations between blue and red types

2.3. aNCI Combined with QM/MM MFEP Simulations. In principle, one can use eqs 2 and 4 to carry out the aNCI analysis for any system with thermal motions. However, some technical problems can make aNCI unfeasible. For instance, all the structures generated by molecular dynamics simulations are required to be aligned based on some criteria such as the minimization of root-mean-square deviations. This alignment process can cause artificial bias in the aNCI analysis. Hence, we partition the entire system into the *subsystem* (that is the targeting region analyzed by aNCI, such as solute in solution) and the *environment* (that is the surrounding regions of the subsystem, such as solvent). The *subsystem* structure is fixed at an optimized structure in the aNCI analysis while the *environment* fluctuates. Therefore, the aNCI analysis needs a representative subsystem structure and an ensemble of structures for fluctuating environment.

Since aNCI is an analysis technique based on given system conformations, it is possible to interface the aNCI analysis with any classical or QM/MM simulation methods. In this work, we incorporate the recently developed quantum mechanics/ molecular mechanics minimum free energy path (QM/MM-MFEP) optimization technique into the aNCI analysis. QM/MM-MFEP has been applied to solvation reactions and enzyme systems[8,17,19,20−22]. In QM/MM-MFEP, the subsystem is described by QM while the environment is simulated by classical force fields. The QM/MM-MFEP optimized structure of the subsystem is ensemble-averaged since the subsystem region is optimized over the potential of mean force surface, which is defined by

$$A(\mathbf{r}_{QM}) = -\frac{1}{\beta} \ln\left(\int d\mathbf{r}_{MM} \exp(-\beta E(r_{QM}, r_{MM}))\right)$$

where $E(\mathbf{r}_{QM}, \mathbf{r}_{MM})$ is the total energy of the entire system expressed as a function of the Cartesian coordinates of the QM and MM subsystems. The QM/MM interaction energy in $E(\mathbf{r}_{QM}, \mathbf{r}_{MM})$ includes the electrostatic interactions from classical point charges and van der Waals (vdW) interactions between QM and MM subsystems. The integration of QM/MM MFEP into the aNCI analysis is efficient and intuitive. The aNCI analysis can also be combined with any other type of molecular dynamics simulation. One just needs to fix the solute molecules at an optimized geometry and carry out the molecular dynamics simulation with the solvent molecules.

3. COMPUTATIONAL DETAILS

We carried out the aNCI analysis on systems that are summarized in Table 1, including single molecule solvation, S_N2 reaction in water, and ligand-protein binding systems. In QM/MM simulations, the subsystem was treated as quantum mechanics at a B3LYP/6-31+G* level.[23] CHARMM22 force field[24] and TIP3P water model[25] were employed for environments. The protein systems were prepared with MolProbity.[26] Each system was optimized by QM/MM-MFEP with a 640 ps simulation. The 320 ps simulations then were performed to generate the snapshots for the aNCI analysis. 1000 snapshots were generated for each system.

The aNCI analysis was carried out with modified version of NCIPLOT software.[12] To reduce the computational cost, the promolecular density[6] from atoms within a 15 Å radius cutoff of the subsystem were chosen to compute the indices using eq 2 and 4. The cube grids, with a 0.05 (if not further mentioned) Å step size along x, y, and z directions, were generated with 3.0 Å buffer regions from the subsystem. In the 3D visualization process with VMD, the threshold for RDG/aRDG was 0.25, and the color scale was [−2, 2], [0, 1.5] for aNCI analysis and fluctuation index, respectively.

4. RESULTS AND DISCUSSION

4.1. Benchmark Study: One Water Molecule in Water.

4.1.1. aRDG Definition: $\overline{s(\mathbf{r})}$ vs $\langle s(\mathbf{r}) \rangle$. To validate two possible definitions for aNCI, we used promolecular density to characterize the noncovalent interactions of one water molecule in water. As shown in Figure 1, $\overline{s(\mathbf{r})}$, defined in eq 2 approaches
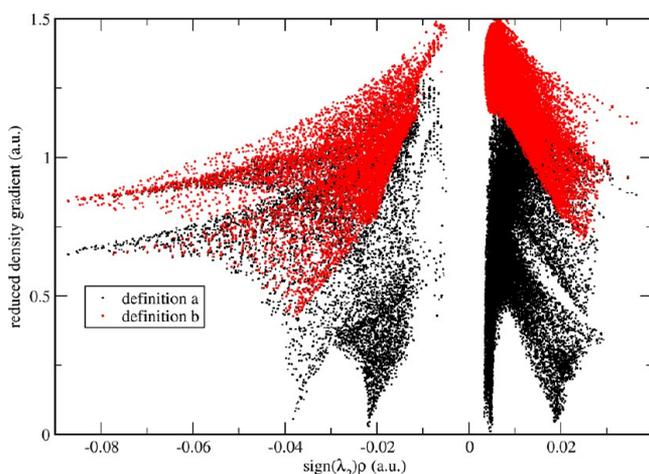

Figure 1. aRDG vs effective density plot under different RDG definitions.

zero at small density regions and the spikes can be clearly identified. In contrast, the $\langle s(\mathbf{r}) \rangle$ defined in eq 3 does not have (close) zero RDG regions and only two spikes can be observed. According to the original NCI paper,[6] such spikes represent noncovalent interaction regions. These indicate that the microscopic details of interactions are lost in $\langle s(\mathbf{r}) \rangle$. This phenomenon can be further explained by a detailed analysis over the RDG distribution. Three 3D grids, located at three ICPs (with effective density as −0.04, −0.02, and 0.005, which will be observed later to correspond with hydrogen bond donor, hydrogen bond acceptor, and vdW regions, respectively) under $\overline{s(\mathbf{r})}$ definition were selected. For each grid, 1000 RDG values were calculated from each snapshot and their distributions are shown in Figure 2. Some interactions were blurred by the broad RDG distribution, although these interactions do exist under averaged density and gradient sense. This suggests that large thermal fluctuations of unstable interactions can bury the useful information of aNCI in $\langle s(\mathbf{r}) \rangle$. Therefore, we chose the definition $\overline{s(\mathbf{r})}$ for our aNCI analysis.

4.1.2. Electron Density: ab Initio vs Promolecular. To examine how promolecular and ab initio electron densities affect the aNCI analysis, we compared the computed RDGs using both electron densities. The ab initio density is constructed using density functional theory calculations with a B3LYP/6-31G* basis set over a small rectangle water box
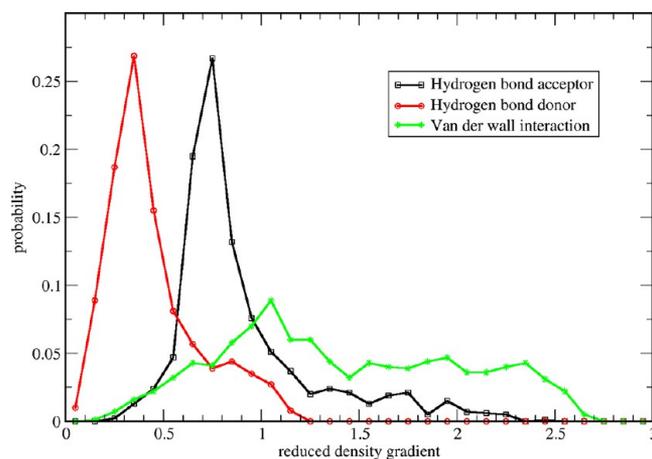

Figure 2. Monitored RDG probability distribution for selected points from three regions: (1) hydrogen bond acceptor, (2) hydrogen bond donor, and (3) van der Waals interaction region.

(around 200 atoms) with 5.0 Å buffer zone to the QM water molecule for each snapshot. As shown in Figure 3, two aRDG
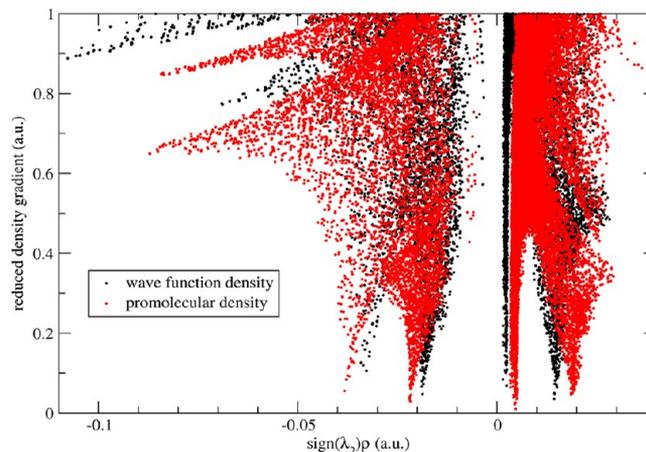

Figure 3. aRDG vs effective density plot for a water molecule in water with promolecular density and wave function density.

plots (black and red dots) against effective density are similar in terms of overall shapes. Furthermore, the absolute electron density at critical points is slightly smaller in ab initio calculations (0.032 and 0.019) than promolecular results (0.039 and 0.021). Therefore, promolecular density is qualitatively accurate to perform the aNCI analysis, which is also confirmed in previous single snapshot NCI analysis.

4.2. Case I: Solute−Solvent Systems.

In Case I, we applied the aNCI analysis to two systems: water in water and benzene in water, which represent prototypical examples of highly fluctuating systems. While the normal NCI analysis shows information about time dependent noncovalent information and so does not reveal solvation interactions (see Figure 5), $\overline{s(\mathbf{r})}$ does. Figure 4 illustrates the evolution of the aRDG as a function of the number of snapshots; 1000 snapshots can achieve the converged aRDG at low-density regions in terms of number and positions of spikes. In the water−water system (Figure 4a), the effective density value at the most negative ICP is −0.06 with 1 snapshot and −0.04 with 10 snapshots and is converged with −0.038 under 100 and 1000 snapshots. In the benzene−water system, the effective
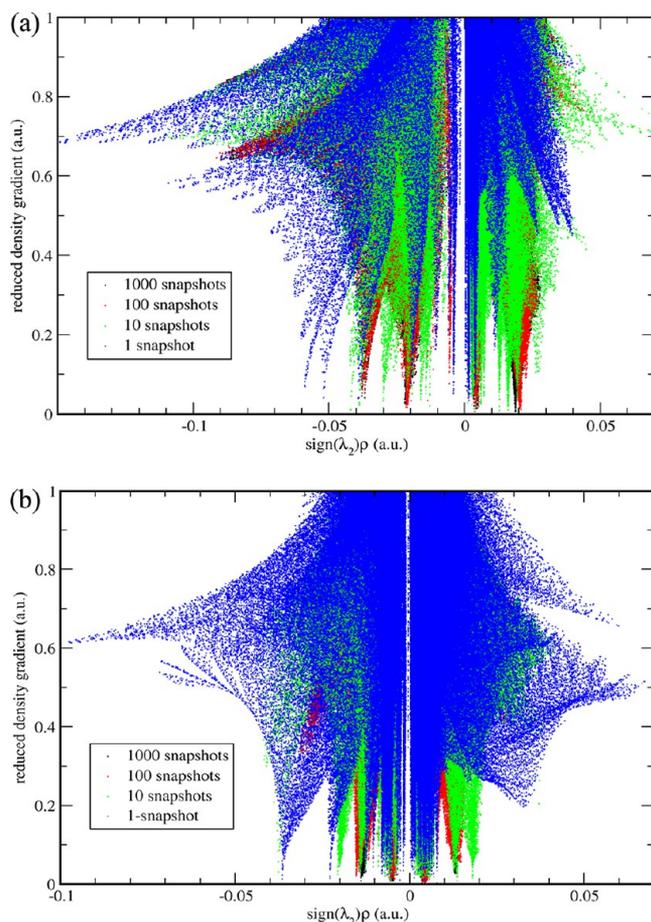
Figure 4. In the (a) water–water system and (b) benzene–water system, (a)RDG vs effective density plot for 1, 10, 100, 1000 snapshots are shown in blue, green, red, and black, respectively.

value at the most negative ICP increases from −0.038 with 1 snapshot to −0.014 with 1000 snapshots. These modifications of ICP's effective density indicate that the use of an ensemble of structures influences the interaction strength. For example, the actual hydrogen bonding would not be as strong as it can be in a single snapshot because fluctuations exist. More importantly, the visualized aNCI pictures can reveal the microscopic solvation structures as shown in Figure 5 for the water–water and benzene–water systems, respectively.

Figure 5a,c represents the single snapshot NCI analysis for both systems. In the NCI analysis, an increased number of weak interactions are observed which results in a nonsymmetrical geometry for the ICP's and in a concealment of the important interactions. They all are averaged out in aNCI calculations. Therefore, in aNCI, the main (or important) interactions are clearly visualized (as shown in Figure 5b,d): water–water hydrogen bond and benzene–water π–hydrogen bond. These comparisons explicitly show that aNCI is required in a fluctuating environment. The detailed interactions of both systems are discussed below.

Water–Water Interactions. Many studies on water structures have been carried out.[27,28] In ideal conditions, water molecules interact with each other through two hydrogen atoms as hydrogen bond donors and oxygen atom as hydrogen bond acceptor. The solute oxygen atom interacts with two other hydrogen atoms from other waters and a tetrahedral hydrogen bond pattern is formed. Both hydrogen bond

donors/acceptors should have the same interaction strength due to its symmetry. The aNCI analysis results, which positions the four hydrogen bond ICPs under tetrahedral shape, are consistent with the experimental symmetry. In addition, the hydrogen bond donor is observed to have larger effective density (−0.037) than the hydrogen bond acceptor (−0.021), with the negative sign indicating that both regions are attractive interactions between *subsystem* and *environment*. When a hydrogen bond network forms, environment water hydrogen atoms can interact with subsystem water oxygen atom from any direction, and this fluctuation is reflected on the decreased density value. As pointed out by Kumar et al.,[29] the average hydrogen bond number per water molecule in liquid state is 3.2−3.6 (less than 4), and this corresponds to the strength decrease of the two hydrogen bond acceptors in our analysis. The aNCI picture is also similar with a spatial position function in the water−water environment as described in ref 30. This demonstrates the advantages of aNCI in revealing the spatial distribution, the interaction type, and the strength.

Benzene−Water Interaction. The benzene−water system has also been studied previously.[31,32] After the interesting π− hydrogen bonding[31,32] was proposed, many theoretical and experimental studies[33−39] have been carried out. The π− hydrogen bonding was found to be at both sides of the benzene ring, and the benzene molecule was shown to act as a hydrogen bond acceptor. The interaction strength was much smaller and more flexible than water−water hydrogen bond networks. The π−hydrogen bond was also found to be highly unstable in nature. In the aNCI analysis, the π−hydrogen bond structure of benzene in 3D space appears clearly for the first time. The overlap between repulsive (effective density 0.013) and attractive (effective density −0.014) contributions have similar nature as the solute water oxygen atom (hydrogen bond acceptor): since the π−hydrogen bonding region is fairly broad, steric clash contributes to the positive effective density value.

The fluctuation indexes of both systems are depicted in Figure 6. For the water−water system, the lowest fluctuations are encountered around the hydrogen bond donor interaction region (0.30%). Therefore, these interactions are mostly stable compared to the hydrogen bond acceptor ones (0.61%). Finally, the vdW interactions appear to be the most flexible ones (∼1.2%). For the benzene−water system, the relative stability of interactions follows: π−hydrogen bonding (0.67%) > benzene planar vdW interaction (0.95%) > close to π− hydrogen bonding vdW interactions (1.3%). In these cases, the stronger the interaction is, the smaller the fluctuations are. It is also obvious that the π−hydrogen bonding is more flexible than all the polar interactions in the water−water system, which is consistent with the experimental observations.[40,41] The fluctuation index is demonstrated to be physical and could be used to analyze the rigidity of different interactions.

4.3. Case II: Solvation Structures during S_N2 Reaction. In this case, the aNCI analysis is used to analyze the solvation effect through simple S_N2 reaction of $Cl^- + CH_3Cl \rightarrow CH_3Cl + Cl^-$. The transition state is taken from a reaction path generated using QM/MM-MFEP, and the reactant state is fully optimized. In Figure 7, the aRDG vs effective density is plotted for both reactant and transition states. The aNCI interactions and its fluctuation index between the *subsystem* and *environment* were visualized in Figure 8.

In Figure 7, along the nucleophile attack toward to the transition state, the spikes are getting narrower and the density of the strongest interactions (both repulsive and attractive)
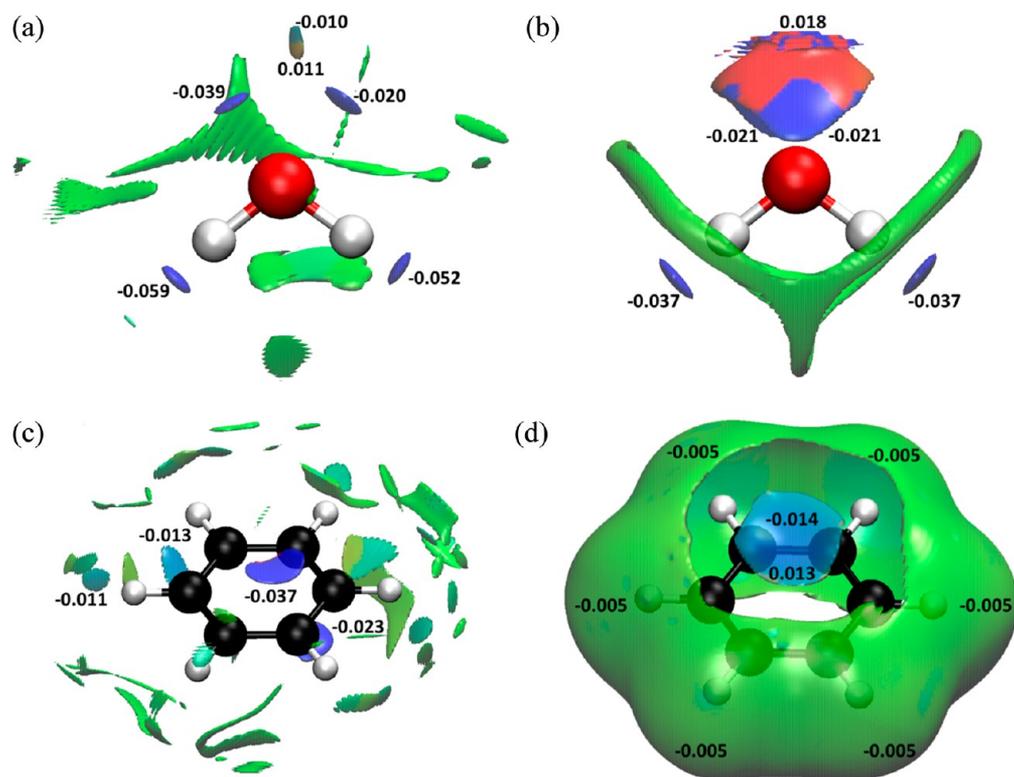
Figure 5. Interactions of water−water and benzene−water systems under 1 snapshots NCI analysis in (a) and (c) and 1000 snapshots aNCI analysis in (b) and (d).
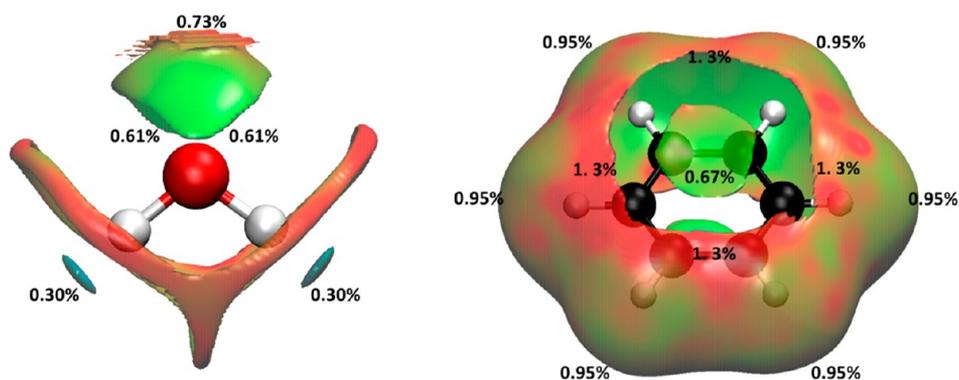

Figure 6. Fluctuation index visualization of water−water and benzene−water systems.

decreases. Both effects may be caused by a rearrangement of the electron density (and therefore the atomic charges) within the subsystem. Indeed, in the reactant state, the charge of the attaching/leaving Cl is −1.0/−0.23 au, respectively, while in the transition state, both of them have −0.71 au and small positive charge migrates on the hydrogen atoms. The surrounding water molecules respond to the substrate charge change, and the radial distribution function (RDF) between Cl and water hydrogen atoms has been plotted in Figure 9. In the transition state, both Cl has a similar RDF with environmental water hydrogen atoms, which is consistent with the charge equity. In the reactant state, the attaching Cl attracts more first shell water hydrogen atoms than the transition state Cl. That indicates that, with a more negative charge, the interactions between the ion−water pair are stronger, and our fluctuation index agrees with the understanding that the stronger interaction is less fluctuating. Although our approach is based on the static solute conformation, a prevoius ab initio molecular dynamics study[42]

on the same system has observed that the static and dynamics approaches have similar global features, and this further validates our conclusion.

4.4. Case III: Ligand−Protein Binding Interactions.
Crystal structures are commonly used to characterize binding pockets and positions of specific ligands to guide drug design. However, a direct observation over crystal structures would be subjective and it could be insufficient to reveal critical binding interactions between ligand and protein. Furthermore, crystal structure is static and may not be helpful to extract binding information. Here, aNCI analysis is applied to analyze the binding patterns of ligand−protein systems.

We chose two ligands in our study. The first one is a preclinical drug molecule, BIIB021.[43−45] It is a small molecule inhibitor of the heat shock protein Hsp90 that binds competitively with geldanamycin in the ATP-binding pocket of Hsp90. The molecular structure is taken from PDB: 3O6O. The second one is an in silico drug design intermediate
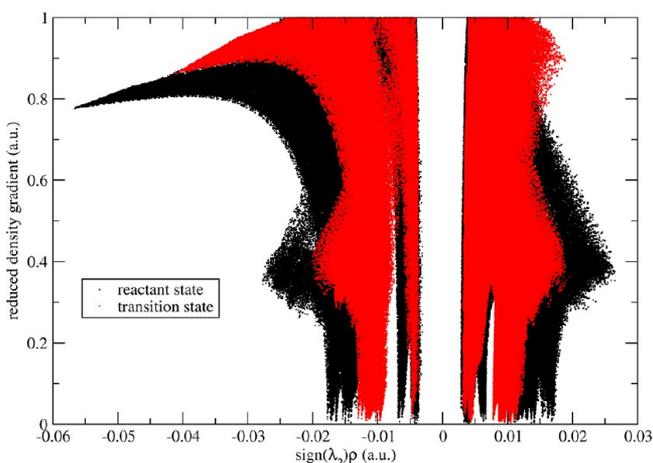
Figure 7. aRDG vs effective density plot in $Cl^- + CH_3Cl$ S_N2 reaction: reactant state (black) and transition state (red).

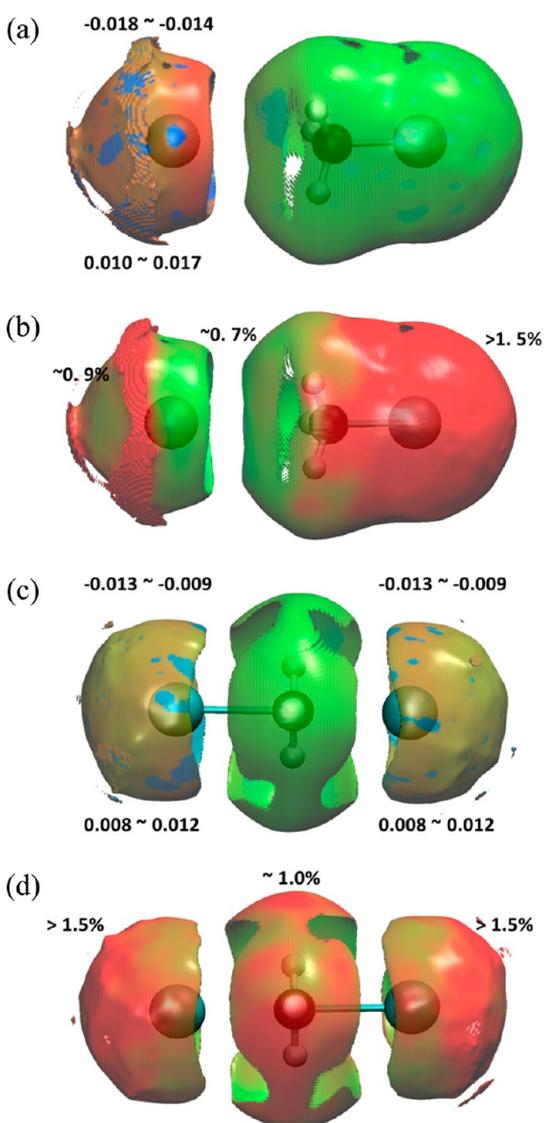**Figure 8.** Reactant and transition state of $Cl^- + CH_3Cl$ S_N2 reaction in water under: reactant state (a) 1000 snapshots aNCI analysis and (b) fluctuation index and transition state (c) 1000 snapshots aNCI analysis and (d) fluctuation index.
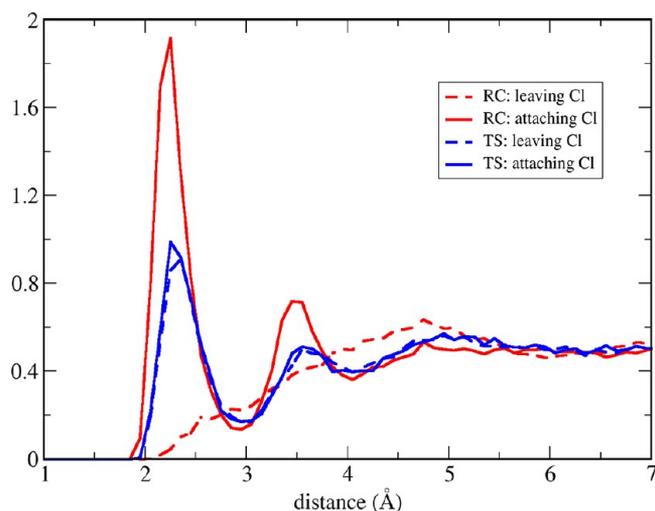

Figure 9. Radial distribution function of Cl and water hydrogen atoms in reactant (RC) and transition (TS) states, for both leaving and attaching Cl atoms.

compound in ligand-protein binding study,[46] named VHD as from structure PDB: 2XAB. Both ligands have a purine scaffold and aromatic moiety. The bound proteins, Hsp83 and Hsp90, have similar global folding and active site structures. The interactions between substrate and environments have been scratches in Figure 10a,b. In both figures, all polar atoms with a distance less than 4.0 Å from the ligand are shown, with no explicit hydrogen atoms.
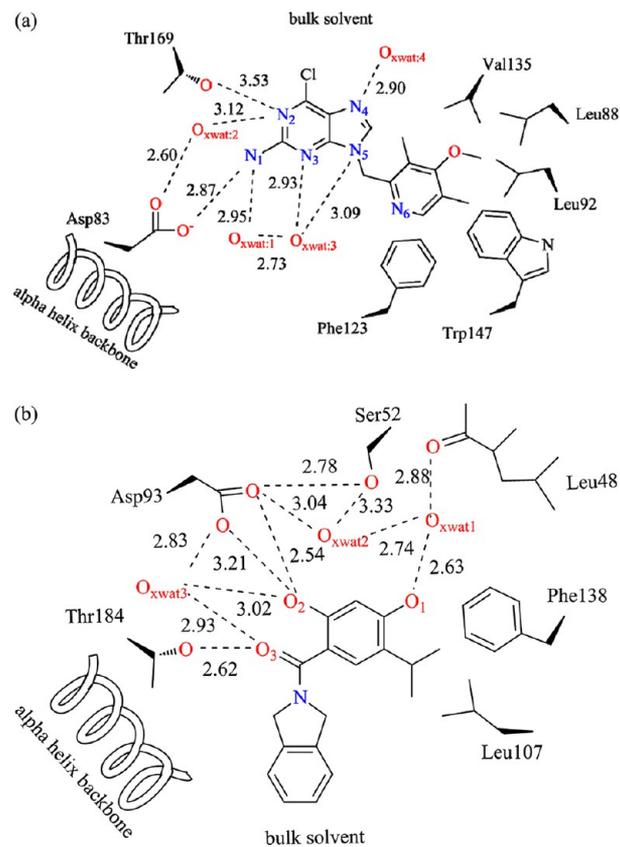

Figure 10. BIIB02 and VHD interactions with environment, according to crystal structure with PDB: 3O6O, 2XAB.

In both systems, the substrate occupies the same active site with different orientations. Two polar amino acids, Asp and Thr, both directly and indirectly interact with the two substrates: BIIB021 over the purine scaffold N_1 and N_2 and VHD over the aromatic moiety O_2 and linkage O_3. Three crystal water molecules were observed inside the active site for both systems, and they are confined in hydrogen bond networks. The BIIB021 aromatic moiety largely locates within the active site and is surrounded by many nonpolar residues: Phe123, Tyr124, Trp147, Leu92, Leu88, and Val135. In contrast, most of the VHD purine part is solvent accessible, which may indirectly stabilize the substrate binding.

To reveal more information based on crystal structures, we carried out QM/MM-MFEP optimization for both systems. The optimized substrate structures have only 0.148 and 0.161 carbon atom root-mean-square-deviation with respect to those in crystal structures, respectively. This indicates that QM/MM-MFEP optimization conserves the ligand binding poses. On the basis of this subsystem structure, the aNCI analysis with 1000 snapshots is calculated. The 3D aNCI density and aNCI fluctuation index for both substrates are shown in Figures 11 and 12, and the ICP effective density and fluctuation index are listed in Tables 2 and 3, respectively.
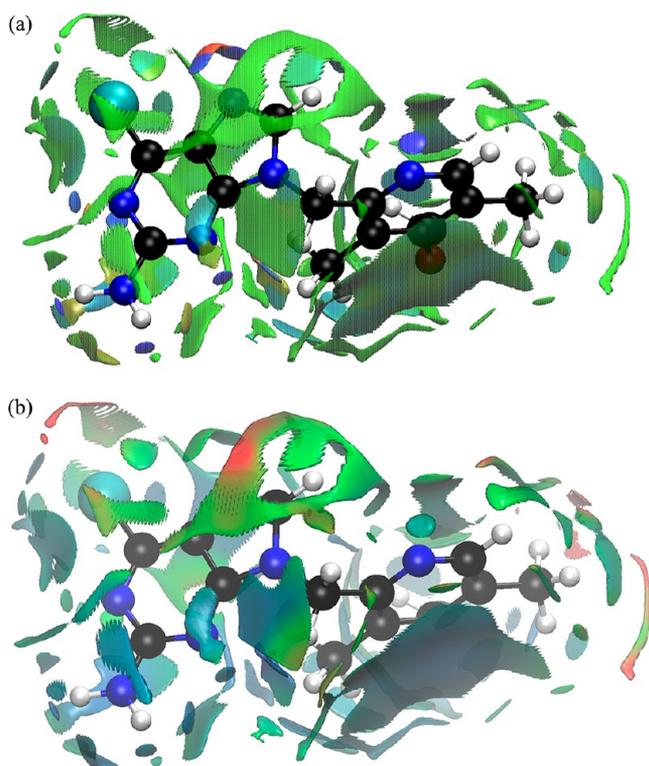

Figure 11. aNCI analysis and fluctuation index of BIIB021 and protein environment under (a) 1000 snapshots aNCI analysis and (b) fluctuation index.

4.4.1. BIIB021 Interaction Features. Polar interactions between BIIB021 and environments are summarized in Table 2 and can be visualized in Figure 11. The two ICPs of the N_1 atom correspond to strong hydrogen bonds (HB) with Asp83 (−0.048) and a crystal water molecule $XWAT_1$ (−0.031). The average HB distances are 1.73 Å and 2.01 Å, respectively. N_2 behaves as the HB acceptor for both Thr169 (−0.016) and $XWAT_1$ (−0.016). A detailed analysis over the 1000 structures

demonstrates that the HB constantly switches between $XWAT_2$-N_2 and Thr169-N_2. This is so frequent that, in average, N_2 shares HBs with both groups. This effective density is about half of the N_1 atom interactions, which goes along with the averaged HB distance between N_2 and $XWAT_2$ (2.62 Å), Thr169-OH group (2.87 Å). N_3 has only one HB with $XWAT_3$ (−0.031), which is consistent with the crystal structure observation. This water position is quite rigid with an averaged HB distance of 2.03 Å. The N_4 atom, which has $XWAT_4$ nearby from crystal structure, forms two directional hydrogen bonds with bulk water molecules (during the MD simulations, several water molecules moved around the N_4 atom and no stable HB exists). This difference between crystal structure observation and aNCI results may be caused by the local environment, which makes water molecules favor a two-side interaction direction, not along the coplane of purine ring. On the other hand, the N_6 atom has only one strong interaction with bulk water molecules, and this is because the local environment around the N_6 atom restricts the bulk water molecules to approach it from this single direction. Besides the aNCI density, the fluctuation index over these hydrogen bonds is observed to be closely related with their interaction strength. For N_2 and N_4, the fluctuation indexes are 0.55%, 0.58% and 0.47%, 0.60%, respectively, and their effective densities are about half comparing with those of N_1 and N_3. The weaker the effective density amount is, which may be caused by interaction with versatile waters, the more flexible these interactions are.

The $\pi-\pi$ stacking between the aromatic moiety and the Phe123 side chain creates the most stable vdW interaction with fluctuation index around 0.25%, which is even less fluctuated than the strongest hydrogen bond. The aromatic moiety ring appears therefore rigid and suitable for substrate binding. The purine ring's interaction with Met83 and Asn36 is also stable, with fluctuation index around 0.35%. However, since the latter are comparably weaker than HBs, the contribution to the substrate binding may be limited.

4.4.2. VHD Interaction Features. The interactions between VHD and environment are listed in Table 3 and visualized in Figure 12. The O_2 atom is tightly bound to Asp93. Asp93 not only directly stabilizes the O_2 atom but also helps to confine the crystal waters $XWAT_2$ and $XWAT_3$. The O_1 atom is hydrogen bonded with $XWAT_1$ which is stabilized by Leu48, and this interaction is the second strongest polar interaction. The O_3 atom has two HBs: one with Thr184, and another with $XWAT_3$, which is stabilized by Asp93. The aNCI analysis is consistent with direct crystal structure observations, and it offers more information on interaction strength and stability.

Besides the polar interactions, the purine-scaffold ring makes a hydrophobic interaction with Ala55 which has an effective density value of −0.009. A hydrophobic interaction between the aromatic ring and Asn51, Ser52 backbone, has a similar strength and confines the substrate inside the active site.

According to our aNCI analysis, the purine scaffold is accessible to bulk solvent and only has fluctuated weak interactions with protein. If the binding mode does not change with the chemical modifications, the C5 atom of purine scaffold could be a promising site. Indeed, as found in experimental studies,[47] modifications over this region help to improve the biological property without disturbing the binding ability. In contrast, the modifications carried out on the aromatic moiety (change of O_1 and isopropanol groups) can dramatically decrease the binding ability.
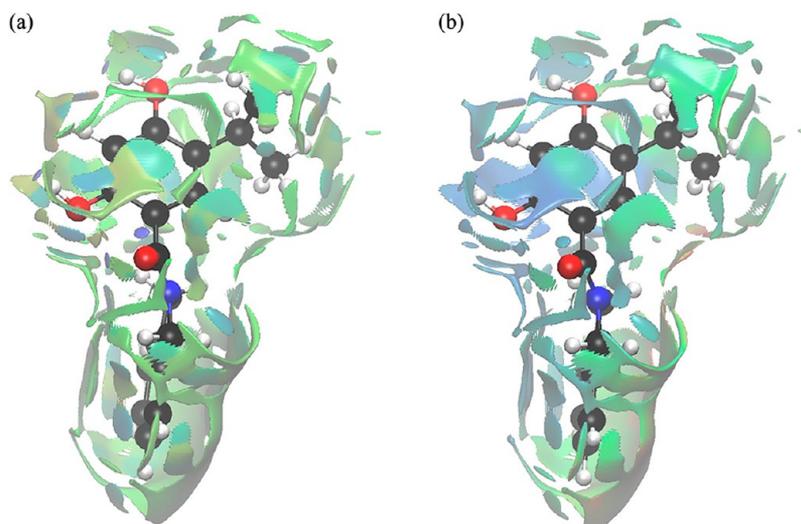
(a) (b)

Figure 12. aNCI analysis and fluctuation index of VHD and protein environment under (a) 1000 snapshots aNCI analysis and (b) fluctuation index.

Table 2. Effective Density and Fluctuation Index of the BIIB021−protein System

	subsystem							
	N_1	N_1	N_2	N_2	N_3	N_4	N_4	N_6
environment	Asp83	$XWAT_1$	Thr169	$XWAT_2$	$XWAT_3$	bulk water	bulk water	bulk water
effective density	−0.048	−0.031	−0.016	−0.016	−0.031	−0.024	−0.018	−0.031
fluctuation index	0.27%	0.35%	0.55%	0.58%	0.34%	0.47%	0.60%	0.40%

Table 3. Effective Density and Fluctuation Index of the VHD−Protein System

	subsystem			
	O_1	O_2	O_3	O_3
environment	$XWAT_1$	Asp93	Thr184	$XWAT_3$
effective density	−0.046	−0.064	−0.046	−0.026
fluctuation index	0.23%	0.17%	0.33%	0.40%

From aNCI analysis, both ligands were observed to bind the protein very well: the BIIB021 utilizes mainly nitrogen atoms to form hydrogen bond with the crystallized water and protein residues; the VHD has three oxygen atoms that form a strong hydrogen bond with environment. The Asp residue is in a crucial role for the binding conformation: it not only forms a direct hydrogen bond with substrate but also helps the creation of an internal water hydrogen bond network. With these confined water molecules, the substrate can bind the active site strongly. A further design for a potential drug molecule would maintain the critical interactions revealed by aNCI while ligand modifications should be performed on those unstable and weak interaction parts.

5. CONCLUSION

In this work, the NCI analysis is generalized to aNCI analysis, which characterizes the interactions from an ensemble of structures. With the aNCI density and aNCI fluctuation index, both averaged noncovalent interactions and fluctuations can be directly visualized. For the solute−solvent system, the tetrahedral hydrogen interaction network in water−water and the π−hydrogen bond in benzene−water system were characterized. The π−hydrogen bond appears as a weaker and more flexible interaction comparing with water−water counterpart. In S_N2 reaction, a reorganization of partial charges changes the solvation structures, and as well as the interaction strengths with environment. Further applications in ligand−protein binding systems reveal the complex interaction networks of two drug molecules in the heat shock protein active site. With aNCI analysis, the crystal structure was further illustrated, and it could help the drug design process.

The aNCI analysis is general and can be coupled with any type of molecular dynamic simulation (QM, QM/MM, polarizable and classical MM force fields). In this work it was interfaced with the recently developed QM/MM-MFEP approach with classical force field. However, in a system difficult to represent by a classical force field, such as metal cations, pure QM or polarizable force fields would play a critical role. Further works are currently ongoing to study the influence of these methods used on the aNCI results. Overall, aNCI is a useful tool to characterize noncovalent interaction patterns in fluctuating environments.

■ **AUTHOR INFORMATION**

Corresponding Author
*E-mail: weitao.yang@duke.edu.

Notes
The authors declare no competing financial interest.

■ **REFERENCES**

(1) Müller-Dethlefs, K.; Hobza, P. *Chem. Rev.* **1999**, *100*, 143−168.

(2) Cerny, J.; Hobza, P. *Phys. Chem. Chem. Phys.* **2007**, *9*, 5291–5303.

(3) Matthews, C. R. *Annu. Rev. Biochem.* **1993**, *62*, 653–683.

(4) Robertson, A. D.; Murphy, K. P. *Chem. Rev.* **1997**, *97*, 1251–1268.

(5) Shuguang, Z. *Nat. Biotechnol.* **2003**, *21*, 1171–1178.

(6) Johnson, E. R.; Keinan, S.; Mori-Sánchez, P.; Contreras-García, J.; Cohen, A. J.; Yang, W. *J. Am. Chem. Soc.* **2010**, *132*, 6498–6506.

(7) Contreras-García, J.; Yang, W.; Johnson, E. R. *J. Phys. Chem. A* **2011**, *115*, 12983–12990.

(8) Wu, P.; Cisneros, G. A.; Hu, H.; Chaudret, R.; Hu, X.; Yang, W. *J. Phys. Chem. B* **2012**, *116*, 6889–6897.

(9) Nilsson Lill, S. O. *Phys. Chem. Chem. Phys.* **2011**, *13*, 16022–16027.

(10) Spackman, M. A.; Maslen, E. N. *J. Chem. Phys.* **1986**, *90*, 2020–2027.

(11) Pendas, A. M.; Luana, V.; Pueyo, L.; Francisco, E.; Mori-Sanchez, P. *J. Chem. Phys.* **2002**, *117*, 1017–1023.

(12) Contreras-García, J.; Johnson, E. R.; Keinan, S.; Chaudret, R.; Piquemal, J.-P.; Beratan, D. N.; Yang, W. *J. Chem. Theory Comput.* **2011**, *7*, 625–632.

(13) van Severen, M.-C.; Chaudret, R.; Parisel, O.; Piquemal, J.-P. *Chem. Phys. Lett.* **2012**, *532*, 9–12.

(14) Beck, E. M.; Hyde, A. M.; Jacobsen, E. N. *Org. Lett.* **2011**, *13*, 4260–4263.

(15) Gillet, N.; Chaudret, R.; Contreras-Garc, J.; Yang, W.; Silvi, B.; Piquemal, J.-P. *J. Chem. Theory Comput.* **2012**, *8*, 3993–3997.

(16) Hu, H.; Yang, W. *Annu. Rev. Phys. Chem.* **2008**, *59*, 573–601.

(17) Hu, H.; Lu, Z.; Yang, W. *J. Chem. Theory Comput.* **2007**, *3*, 390–406.

(18) Humphrey, W.; Dalke, A.; Schulten, K. *J. Mol. Graphics* **1996**, *14*, 33–38.

(19) Hu, H.; Lu, Z.; Parks, J. M.; Burger, S. K.; Yang, W. *J. Chem. Phys.* **2008**, *128*, 034105–034123.

(20) Parks, J. M.; Hu, H.; Rudolph, J.; Yang, W. *J. Phys. Chem. B* **2009**, *113*, 5217–5224.

(21) Zeng, X.; Hu, H.; Hu, X.; Yang, W. *J. Chem. Phys.* **2009**, *130*, 164111–164119.

(22) Hu, X.; Hu, H.; Melvin, J. A.; Clancy, K. W.; McCafferty, D. G.; Yang, W. *J. Am. Chem. Soc.* **2010**, *133*, 478–485.

(23) Lee, C.; Yang, W.; Parr, R. G. *Phys. Rev. B* **1988**, *37*, 785–789.

(24) MacKerell, A. D.; Bashford, D.; Bellott, M.; Dunbrack, R. L.; Evanseck, J. D.; Field, M. J.; Fischer, S.; Gao, J.; Guo, H.; Ha, S.; Joseph-McCarthy, D.; Kuchnir, L.; Kuczera, K.; Lau, F. T. K.; Mattos, C.; Michnick, S.; Ngo, T.; Nguyen, D. T.; Prodhom, B.; Reiher, W. E.; Roux, B.; Schlenkrich, M.; Smith, J. C.; Stote, R.; Straub, J.; Watanabe, M.; Wiórkiewicz-Kuczera, J.; Yin, D.; Karplus, M. *J. Phys. Chem. B* **1998**, *102*, 3586–3616.

(25) Jorgensen, W. L.; Chandrasekhar, J.; Madura, J. D.; Impey, R. W.; Klein, M. L. *J. Chem. Phys.* **1983**, *79*, 926–935.

(26) Davis, I. W.; Leaver-Fay, A.; Chen, V. B.; Block, J. N.; Kapral, G. J.; Wang, X.; Murray, L. W.; Arendall, W. B.; Snoeyink, J.; Richardson, J. S.; Richardson, D. C. *Nucleic Acids Res.* **2007**, *35*, W375–W383.

(27) Head-Gordon, T.; Hura, G. *Chem. Rev.* **2002**, *102*, 2651–2670.

(28) Clark, G. N. I.; Cappa, C. D.; Smith, J. D.; Saykally, R. J.; Head-Gordon, T. *Mol. Phys.* **2010**, *108*, 1415–1433.

(29) Kumar, R.; Schmidt, J. R.; Skinner, J. L. *J. Chem. Phys.* **2007**, *126*, 204107–204119.

(30) Sharp, K. A.; Vanderkooi, J. M. *Acc. Chem. Res.* **2009**, *43*, 231–239.

(31) Atwood, J. L.; Hamada, F.; Robinson, K. D.; Orr, G. W.; Vincent, R. L. *Nature* **1991**, *349*, 683–684.

(32) Suzuki, S.; Green, P. G.; Bumgarner, R. E.; Dasgupta, S.; Goddard, W. A.; Blake, G. A. *Science* **1992**, *257*, 942–945.

(33) Gierszal, K. P.; Davis, J. G.; Hands, M. D.; Wilcox, D. S.; Slipchenko, L. V.; Ben-Amotz, D. *J. Chem. Phys. Lett.* **2011**, *2*, 2930–2933.

(34) Bondesson, L.; Rudberg, E.; Luo, Y.; Sałek, P. *J. Comput. Chem.* **2008**, *29*, 1725–1732.

(35) Allesch, M.; Lightstone, F. C.; Schwegler, E.; Galli, G. *J. Chem. Phys.* **2008**, *128*, 014501–014510.

(36) Allesch, M.; Schwegler, E.; Galli, G. *J. Phys. Chem. B* **2007**, *111*, 1081–1089.

(37) Giuseppe, G. *Chem. Phys. Lett.* **2006**, *429*, 114–118.

(38) Baron, M.; Kowalewski, V. J. *J. Phys. Chem. A* **2006**, *110*, 7122–7129.

(39) Schravendijk, P.; van der Vegt, N. F. A. *J. Chem. Theory Comput.* **2005**, *1*, 643–652.

(40) Zheng, J.; Kwak, K.; Asbury, J.; Chen, X.; Piletic, I. R.; Fayer, M. D. *Science* **2005**, *309*, 1338–1343.

(41) Rosenfeld, D. E.; Kwak, K.; Gengeliczki, Z.; Fayer, M. D. *J. Phys. Chem. B* **2010**, *114*, 2383–2389.

(42) Joubert, L.; Pavone, M.; Barone, V.; Adamo, C. *J. Chem. Theory Comput.* **2006**, *2*, 1220–1227.

(43) Lundgren, K.; Zhang, H.; Brekken, J.; Huser, N.; Powell, R. E.; Timple, N.; Busch, D. J.; Neely, L.; Sensintaffar, J. L.; Yang, Y.-c.; McKenzie, A.; Friedman, J.; Scannevin, R.; Kamal, A.; Hong, K.; Kasibhatla, S. R.; Boehm, M. F.; Burrows, F. J. *Mol. Cancer Ther.* **2009**, *8*, 921–929.

(44) Böll, B.; Eltaib, F.; Reiners, K. S.; von Tresckow, B.; Tawadros, S.; Simhadri, V. R.; Burrows, F. J.; Lundgren, K.; Hansen, H. P.; Engert, A.; Pogge von Strandmann, E. *Clin. Cancer Res.* **2009**, *15*, 5108–5116.

(45) Taldone, T.; Gozman, A.; Maharaj, R.; Chiosis, G. *Curr. Opin. Pharmacol.* **2008**, *8*, 370–374.

(46) Murray, C. W.; Carr, M. G.; Callaghan, O.; Chessari, G.; Congreve, M.; Cowan, S.; Coyle, J. E.; Downham, R.; Figueroa, E.; Frederickson, M.; Graham, B.; McMenamin, R.; O'Brien, M. A.; Patel, S.; Phillips, T. R.; Williams, G.; Woodhead, A. J.; Woolford, A. J. A. *J. Med. Chem.* **2010**, *53*, 5942–5955.

(47) Woodhead, A. J.; Angove, H.; Carr, M. G.; Chessari, G.; Congreve, M.; Coyle, J. E.; Cosme, J.; Graham, B.; Day, P. J.; Downham, R.; Fazal, L.; Feltell, R.; Figueroa, E.; Frederickson, M.; Lewis, J.; McMenamin, R.; Murray, C. W.; O'Brien, M. A.; Parra, L.; Patel, S.; Phillips, T.; Rees, D. C.; Rich, S.; Smith, D.-M.; Trewartha, G.; Vinkovic, M.; Williams, B.; Woolford, A. J. A. *J. Med. Chem.* **2010**, *53*, 5956–5969.